Elastic electron transmission by barriers in a three-dimensional model quantum wire

Xin Ma and Donald J. Kouri
Department of Chemistry and Department of Physics, University of Houston, Houston, Texas 77204-5641

Marshall Luban
Department of Physics and Astronomy and Ames Laboratory, Iowa State University, Ames, Iowa 50011

Naresh Nayar and David K. Hoffman
Department of Chemistry and Ames Laboratory, Iowa State University, Ames, Iowa 50011
(Received 12 October 1992; revised manuscript received 18 December 1992)

Numerical solutions of the time-dependent and time-independent Schrödinger equations for electron tunneling in a three-dimensional model quantum wire have been carried out and used to calculate transmission probabilities over a range of energies. The model simulates a quantum heterostructure corresponding to a cylindrically symetric wire constructed from two different materials such that square barriers to the axial (z) motion occur in the disjoint region $B=(z_1\le z\le z_2)\cup(z_3\le z\le z_4)$. In addition, the electron is bound harmonically in the radial distance r transverse to the longitudinal axis z; the electron vibrational frequency changes discontinuously from ω_A in the disjoint region $A=(-\infty<z<z_1)\cup(z_2<z<z_3)\cup(z_4<z<\infty)$ to ω_B in the disjoint region B. A basis-set expansion, using harmonic-oscillator eigenstates appropriate to regions A or B, for the electron's radial vibration transverse to the cylinder axis is used. The basis-set expansion using the eigenstates of the electrons rotation about z only involved the ground rotational state since, due to cylindrical symmetry, the electron does not experience any torques. This "close-coupling expansion" procedure yields close-coupled-wave-packet (CCWP) equations for the time-dependent expansion coefficients in the time-dependent approach, and a system of linear algebraic equations for the expansion coefficients in the time-independent approach. The change of electronic vibration frequency from region A to region B leads to nonadiabatic transitions, giving rise to transmission amplitudes that depend on the final electron-vibrational state. The model is elastic in that phonon degrees of freedom are not included. A final-state analysis for the time-dependent CCWP method is given which does not require spatial integrals of the wave packets. This enables results over a broad energy range (including resonant energies) to be acquired from a single wave-packet propagation, because the packet is initially taken to be relatively narrow in coordinate space. The method is extremely stable over the whole range of energies. All calculations used an initial state comprised of the ground vibrational and zero angular momentum wave functions and vibrationally resolved transmission probabilities are studied for various frequency ratios ω_A/ω_B and as a function of total energy. Vibrational nonadiabaticity is found to depend strongly of the frequency ratio, and on collision energy.

I. INTRODUCTION

The reduction in size and concomitant increase in the number of circuit elements of transistors has been central to the remarkable reduction in the cost of computers and their enormous increases in computational and logical operations speed.[1] Although there is great motivation to continue this size reduction, microchips have now reached micrometer dimensions and further size reduction will involve devices with dimensions on the same scale as the de Broglie wavelength of the electrons. This implies that the fundamental quantum-mechanical nature of the electrons (quantum tunneling through potential or dynamical barriers) will dominate the behavior of such devices.[2–5] The size regime of these devices ("nanostructure") ranges from ten to a few thousand Å. In this size regime, the wave mechanical properties of electrons require a radically different device design from that employed in present day transistors.[1,4–6]

Important developments for such devices have already been achieved, including the demonstration of quantum coupled devices, demonstration of resonant tunneling devices, beginning fabrication of rudimentary integrated circuits based on resonant electron tunneling, and initial theoretical modeling of resonant electron tunneling and of quantum transport equations in idealized one-dimensional systems.[1,2,7–13] The models attempt to simulate three-dimensional structures which are composed of layers of various semiconducting materials (with different band gaps), with confinement in the two lateral dimensions. The semiconductor materials are layered so that passage along the longitudinal axis requires tunneling through barriers created by juxtaposing high-band-gap semiconductors with low-band-gap semiconductors. The materials are arranged so that tunneling is miniscule except at certain energies, for which the electrons resonantly tunnel.[1–5]

Because the basic mechanism on which the new devices

will function is resonant quantum tunneling, existing models used in developing efficient chip design[6] are not applicable, and new models are needed. In this paper, we take the initial steps in developing reliable computational tools for solving for electron reflection and transmission coefficients as a function of energy and "internal" electron states (i.e., electron vibration and rotation) in a fully three-dimensional physical model representing a nanostructure with two-dimensional lateral containment. The model is kept relatively uncomplicated by using an electron potential-energy function which is the sum of a cylindrically symmetric harmonic-oscillator potential, which gives rise to confinement of the electron transverse to the system axis, and a double-barrier potential corresponding to two segments of semiconductor B juxtaposed to three segments of semiconductor A. The frequencies of the harmonic-oscillator potentials for segments A and B can be chosen to differ, so that vibrational nonadiabatic effects on electron transmission may be studied. In this work, only states with zero angular momentum are considered. Ultimately, the model will be used to study the effects of angular momentum on electron transmission. The model can also be extended to include other types of effects such as angular anisotropy in the confining potential as well as interactions with lattice phonons. The time-dependent approach can also be employed for solutions of the von Neumann equation for the density matrix, permitting more general systems to be studied.

Two distinct approaches are used here to calculate the transmission probabilities. One is an extension to three dimensions of the usual time-independent, boundary matching (BM) or transfer-matrix approach for solving one-dimensional (1D) tunneling problems; the wave function and its derivative along the z axis must be continuous for all finite discontinuities in the potential and the transverse dependence of the wave function is treated by a basis-set expansion using the vibrational-rotational eigenstates in plane polar coordinates (termed a "close-coupling" expansion). Because of symmetry with respect to rotation around the axis of the wire, no coupling occurs between the rotational states. Sufficient oscillator states are included to ensure convergence of the transmission amplitudes and concomitant probabilities. The time-independent problem thus reduces to one of linear algebra.

In addition, we carry out a solution of time-dependent Schrödinger equation by explicitly propagating a wave packet[14–19] using the symmetric split-operator approach.[14–16] The initial packet is taken to be a Gaussian in the z dependence, multiplied by the ground rotational-vibrational initial eigenstate. By choosing an initial wave packet narrow in configuration space, propagation of a single wave packet yields results over a wide range of energies.[19] This is made possible by a new procedure for carrying out the final-state analysis for Cartesian-coordinate propagations, in which the translation variable extends over $(-\infty,\infty)$. The coupling potential matrix, which leads to electron-vibrational transitions, can be obtained analytically, and the dependence of the coupling on the ratio of the harmonic frequencies in regions A and B analyzed in order to understand its effect on the transmission probability.

This paper is organized as follows. In Sec. II we give the formulation of the model and the relevant equations to be solved, including a new procedure for extracting the state-resolved transmission amplitudes from the wave packet. In Sec. III we present and discuss the results obtained. Section IV contains our conclusions.

II. FORMULATION OF THE PROBLEM, SOLUTION METHODS, AND FINAL-STATE ANALYSIS

The Hamiltonian operator for the model problem can be written in cylindrical polar coordinates as

$$H=\frac{-\hbar^2}{2\mu}\left[\frac{\partial^2}{\partial r^2}+\frac{1}{r}\frac{\partial}{\partial r}+\frac{1}{r^2}\frac{\partial^2}{\partial\varphi^2}+\frac{\partial^2}{\partial z^2}\right]+V(z,r)\ , \quad (1)$$

where the potential is given by

$$V(z,r)=\begin{cases}\frac{1}{2}\mu\omega_A^2 r^2\ , & z\in A \quad (2a)\\ \frac{1}{2}\mu\omega_B^2 r^2+V_0\ , & z\in B\ , \quad (2b)\end{cases}$$

with

$$A=(-\infty,z_1)\cup(z_2,z_3)\cup(z_4,\infty)\ , \quad (3)$$

$$B=(z_1,z_2)\cup(z_3,z_4)\ , \quad (4)$$

$$z_1<z_2<z_3<z_4\ . \quad (5)$$

The potential is shown in Fig. 1. For simplicity, we assume a uniform effective electron mass. This Hamiltonian models a nanostructure in which semiconductor A comprises the (disjoint) region A, with semiconductor B spliced in the regions (z_1,z_2) and (z_3,z_4). The (constant)

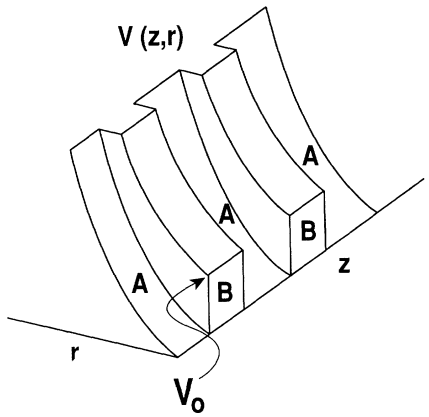

FIG. 1. The potential energy is shown in perspective. The potential is piecewise constant in z, with discontinuous changes occurring as one passes from material A to B at $z=z_1$, B to A at $z=z_2$, A to B at z_3, and finally, B back to A at z_4. The electron is bound in a parabolic potential in its radial distance from the axis of the wire, with the harmonic frequency changing discontinuously at the boundaries between materials A and B.

potential V_0 reflects the different band gap of material B compared to material A. With $\omega_A \neq \omega_B$, the harmonic binding of the electron transverse to the z axis changes discontinuously when one moves from region A to region B and from B to A. Because the potential is independent of φ (cylindrical symmetry), but r and z are not separable everywhere, a solution of the time-independent Schrödinger equation can be constructed as the product of the electron-rotational eigenstate, characterized by the magnetic quantum number m (taken to the $m=0$ ground rotational state) and a function of r and z. The values of the various parameters used in the present simulations are given in Table I. They are chosen to correspond to what is actually feasible to fabricate by molecular-beam-epitaxy (MBE) methods. The parabolic potentials in regions A and B permit the electron to make excursions which are limited in extent by the regions in which the first few harmonic-oscillator wave functions are significantly different from zero. This can be estimated to be about $8a_A$ and $8a_B$ for the two regions, where a is the length scale for a harmonic oscillator, given by $(\hbar/m\omega)^{1/2}$. As seen in Table I, using the bare electron mass and the chosen values of ω_A and ω_B, one gets 0.159 μm for the "A" and 0.138 μm for the "B" semiconductors. These do correspond to reasonable dimensions that can be achieved experimentally. This remains true for the range of ω_A and ω_B used in studies of the effects of the ω_A/ω_B ratio. The total length of the wire is 25 000 Å, or 2.5 μm, again well within the range achievable by MBE. The barrier height V_0, corresponds to a temperature of 45 K, which again seems well within the regime of interest to experiment. Finally, the parameters used in our simulation for the barrier lengths, each taken to be 70 Å or 0.007 μm, can also be fabricated (they can go down to about 10 Å). Thus, we conclude that the model chosen for our simulation has relevance for experimentally realizable systems.

TABLE I. Parameters.

Range of grid (Å)	$(-11\,945, 11\,945)$
No. of grid points	8192
V_0 (eV)	3.837×10^{-3} (=45 K)
ω_A (sec^{-1})	2.914×10^{11}
ω_B (sec^{-1})	3.886×10^{11}
N[a]	10
z_0 (Å)	−2000.0
σ (Å)	200.0
$\bar{k}$ (Å^{-1})	2.244×10^{-2}
Time-step size (sec)	1.00×10^{-15}
Number of steps[b]	38 506
$\lvert z_2-z_1\rvert=\lvert z_4-z_3\rvert$	70 Å
a_A	0.159 μm
a_B	0.138 μm

[a]Convergence studies were carried out including up to 15 vibrational eigenstates, and it was found that satisfactory results were obtained over the entire range of energies with $N=10$.

[b]Both the transmission coefficients and the wave packet in the region of the potential well were monitored to ensure that the propagation was carried out long enough for resonances to decay completely.

The time-dependent propagation involves the formal solution

$$|\psi(t+\tau|n_0m_0)\rangle=\exp(-iH\tau/\hbar)|\psi(t|n_0m_0)\rangle\ , \tag{6}$$

where in all our studies we take the initial electron vibrational quantum number n_0 and magnetic quantum number m_0 to be zero. For convenience (since there can be no rotational transitions) we suppress the m_0. Because of the simplicity of the potential, it is convenient to introduce the above-mentioned close-coupling expansion, so that the wave function in both the time-independent and time-dependent methods becomes a vector whose components are functions of z or of z and t. These are the channel components of the time-independent wave function, or channel wave packets[19] of the time-dependent wave packet. In the latter case, the vibrational eigenfunction expansion avoids having a two-dimensional grid for the wave packet, and because the coupling producing vibrational inelasticity is not too strong, the computational effort is reduced.

It is of interest to compare the above time-independent procedure to that recently developed and applied to a similar model nanostructure by Bryant.[20] In that work, the Cartesian coordinates x, y, and z are used, rather than our cylindrical coordinates r, θ, and z. However, excitation of electronic lateral vibration also results from discontinuous changes in the harmonic force constants for the different regions of the nanostructure. The time-independent method employed by Bryant is the same as is used in the present work; namely, imposition of continuity of the wave function and its longitudinal derivative, combined with the usual imposition of scattering boundary conditions in the "field-free regions." This leads to linear, inhomogeneous algebraic equations to be solved. Bryant does consider a more general model in that he includes the effects of "tapering" of the wire leads that attach to the double-barrier (quantum-well) structure. Our model corresponds to Bryant's "abrupt constriction" case.[20] We now turn to describe the computational schemes.

A. Time independent solution

The Schrödinger equation may be written as

$$H\psi(n_0,E)=E\psi(n_0,E)\ , \tag{7}$$

and in regions A and B $\psi(n_0,E)$ will be expanded in terms of electron-vibrational (harmonic-oscillator) eigenstates, $X_n(\rho)$ appropriate to each region, given by

$$X_n(\rho)=\sqrt{2\mu\omega/\hbar}\exp(-\rho/2)L_n(\rho)\ , \tag{8}$$

satisfying

$$\left[-\frac{\hbar^2}{2\mu}\left[\frac{d^2}{dr^2}+\frac{1}{r}\frac{d}{dr}\right]+\frac{\mu}{2}\omega^2r^2\right]X_n(\rho) =(2n+1)\hbar\omega X_n(\rho)\ , \tag{9}$$

$$\rho \equiv \mu\omega r^2/\hbar \ . \tag{10}$$

The function $L_n(\rho)$ is the Laguerre polynomial, and the $X_n(\rho)$ are normalized so that

$$\int_0^\infty dr\, rX_m(\rho)X_n(\rho)=\delta_{nm} \ . \tag{11}$$

Clearly, two distinct bases result, depending on ω_A and ω_B. We define the transform $\underline{A}$ (an overlap matrix) between these two orthonormal basis sets, so that (for finite N)

$$[X_0(\rho_A),\ldots,X_N(\rho_A)]=[X_0(\rho_B),\ldots,X_N(\rho_B)]\underline{A} \ , \tag{12}$$

and it is easily shown that

$$\begin{aligned}(\underline{A})_{mn} &\equiv \langle X_m(\rho_B)|X_n(\rho_A)\rangle \\ &= \frac{(-1)^m 2\sqrt{\omega_A\omega_B}(m+n)!}{m!n!(\omega_A+\omega_B)} \\ &\quad \times \gamma^{m+n}F[-m,-n;-(m+n),1/\gamma^2] \ .\end{aligned} \tag{13}$$

In Eq. (13), m and n range from 0 up to N,

$$\gamma \equiv \frac{\omega_B-\omega_A}{\omega_B+\omega_A} \ , \tag{14}$$

and F is a hypergeometric function.[21] We take the same basis size, $N+1$, in regions A and B, so the transformation between the two bases is square. We note that the matrix $\underline{A}$ is a basis transformation and therefore is unitary (provided the complete set of quantum states in regions A and B is included). The expansion in region A or B of the casual time-independent solution [denoted by $\psi^+(z,n_0,E)$] is written as

$$\psi^+(z,n_0,E)=\sum_{n=0}^{N}\psi_n^+(z,n_0,E)X_n(\rho_C) \ , \tag{15}$$

where C denotes either region A or B. The total number of basis functions, $N+1$, is determined by testing the results with respect to their stability to a further increase in N. (This is the standard procedure used to ensure convergence of such close-coupling expansions.[19]) We found that $N=10$ results are converged to within a few percent. It is convenient to use a vector notation, so that

$$\begin{aligned}&\psi^+(z,n_0,E) \\ &\quad =[\psi_0^+(z,n_0,E),\psi_1^+(z,n_0,E),\ldots,\psi_N^+(z,n_0,E)]^T \ ,\end{aligned} \tag{16}$$

where the superscript T denotes the transpose. The vector $\psi^+(z,n_0,E)$ satisfies the matrix Schrödinger equation

$$(\underline{H}-\underline{I}E)\psi^+=0 \ , \tag{17}$$

with

$$\underline{H}=\underline{I}\left[-\frac{\hbar^2}{2\mu}\frac{\partial^2}{\partial z^2}\right]+V(z) \ , \tag{18}$$

where $\underline{I}$ is the identity matrix in the $(N+1)\times(N+1)$ space, and

$$V(z)=\begin{cases}\underline{V}_A \ , & z\in A \qquad (19a)\\ \underline{V}_B+V_0\underline{I} \ , & z\in B \ . \qquad (19b)\end{cases}$$

The (constant in z) matrices $\underline{V}_A$ and $\underline{V}_B$ are given by

$$(\underline{V}_A)_{mn}=(2n+1)\hbar\omega_A\delta_{mn} \tag{20}$$

and

$$(\underline{V}_B)_{mn}=\sum_{n'=0}^{N}(2n'+1)\hbar\omega_B(\underline{A})_{m,n'}(\underline{A})_{nn'} \ , \tag{21}$$

with $\underline{A}$ given by Eq. (13).

It is necessary, for the time-independent approach, to explicitly impose the causal boundary conditions to extract the transmission and reflection amplitudes, in terms of which the transmission and reflection probabilities may be computed. We require the components of $\psi^+(z,n_0,E)$ to satisfy

$$\psi_n^+(z,n_0,E)=\begin{cases}\delta_{nn_0}\exp(ik_nz)+r(n,n_0)\exp(-ik_nz) \ , \\ \qquad\qquad z\in(-\infty,z_1) \qquad (22a)\\ t(n,n_0)\exp(ik_nz) \ , \quad z\in(z_4,\infty) \ , \qquad (22b)\end{cases}$$

with

$$k_n=\sqrt{2\mu[E-(2n+1)\hbar\omega_A]}/\hbar \ . \tag{23}$$

The $t(n,n_0)$ is the transmission amplitude where the electron is initially in vibrational state n_0 and finally in vibrational state n, after having completely traversed the B region, and $r(n,n_0)$ is the analogous reflection amplitude for which the reflected electron ends up in vibrational state n. The corresponding transmission and reflection probabilities are given by

$$T(n,n_0,E)=\frac{k_n}{k_{n_0}}|t(n,n_0)|^2 \tag{24}$$

and

$$R(n,n_0,E)=\frac{k_n}{k_{n_0}}|r(n,n_0)|^2 \ , \tag{25}$$

where

$$(2n'+1)\hbar\omega_A<E \tag{26}$$

for both $n'=n$ and n_0. The conservation of probability implies that

$$\sum_{n=0}^{n_{\max}}[T(n,n_0,E)+R(n,n_0,E)]=1 \ , \tag{27}$$

and $n_{\max}$ is the largest value of n' satisfying Eq. (26). For $n>n_{\max}$, the corresponding $\psi_n^+(z,n_0,E)$ are real and

therefore contribute zero reflected or transmitted flux. The behavior of the $\psi_n^+(z,n_0,E)$ in the interior region (z_1,z_4) is determined by requiring that the $\psi_n^+(z,n_0,E)$ and their derivatives $(\partial\psi^+/\partial z)(z,n_0,E)$, be continuous at the points of (finite) discontinuity in the potential, $z=z_1,z_2,z_3,z_4$. Then the procedure for obtaining the transmission and reflection amplitudes $t(n,n_0)$ and $r(n,n_0)$ involves setting up and solving the resulting linear, simultaneous nonhomogeneous algebraic equations. This is, of course, a straightforward matrix generalization of the well-known procedure for solving for the transmission amplitude t and reflection amplitude r for the 1D scattering of an electron by a barrier. However, the double-barrier, additional electron vibrational degree of freedom and the change in oscillator frequency between regions A and B (which causes transitions between vibrational states of the electron while conserving the total electron energy) make the details of the analysis substantially messier, and we simply quote results without going into details. It is easy (although tedious) to show that the transmission and reflection amplitudes in Eqs. (22a) and (22b) are given in terms of matrices

$$\underline{M}_j=\frac{1}{2}\begin{bmatrix} A_{mn}(1-ig_m/k_n)\exp(g_mz_j-ik_nz_j) & A_{nm}(1+ig_m/k_n)\exp(-g_mz_j-ik_nz_j) \\ A_{mn}(1+ig_m/k_n)\exp(g_mz_j+ik_nz_j) & A_{nm}(1-ig_m/k_n)\exp(-g_mz_j+ik_nz_j)\end{bmatrix}, \tag{28}$$

where each "block" has dimension $(N+1)\times(N+1)$, and the matrix $\underline{M}_j$ is obtained by the continuity conditions at z_j, $j=1-4$. The wave numbers g_m are given by

$$g_m=\{2\mu[(2m+1)\hbar\omega_B+V_0-E]\}^{1/2}/\hbar\ , \tag{29}$$

where for open channels for which the kinetic energy [which is $E-(2m+1)\hbar\omega_B$] is greater than V_0 the above expression will yield $i|g_m|$, and for open channels where the kinetic energy is less than V_0 g_m is positive definite. For closed channels, g_m is also positive definite. We use the $\underline{M}_j$ to construct the matrix $\underline{M}$,

$$\underline{M}=\underline{M}_1\underline{M}_2^{-1}\underline{M}_3\underline{M}_4^{-1}\ , \tag{30}$$

which can also be written in the block form

$$\underline{M}=\begin{bmatrix}\underline{M}_{11} & \underline{M}_{12}\\ \underline{M}_{21} & \underline{M}_{22}\end{bmatrix}, \tag{31}$$

with each block again of dimension $(N+1)\times(N+1)$. Then the transmission and reflection amplitudes are given by

$$(\underline{t})_{nn_0}=(\underline{M}_{11}^{-1})_{nn_0} \tag{32}$$

and

$$(\underline{r})_{nn_0}=(\underline{M}_{21}\underline{t})_{nn_0}\ . \tag{33}$$

Thus, one simply constructs the four "connection" matrices $\underline{M}_j$, and from them the matrix $\underline{M}$, to obtain the blocks $\underline{M}_{11}$ and $\underline{M}_{21}$. This provides all the information to calculate the $t(n,n_0)$ and $r(n,n_0)$ once $\underline{M}_{11}^{-1}$ is computed. This completes the method used to solve the time-independent Schrödinger equation.

B. Time-dependent solution

In analogy to the expansion of the time-independent wave function in the bases $X_n(\rho_C)$, Eq. (15), we may also expand $\psi(z,r,n_0,t)$ according to

$$\psi(z,r,n_0,t)=\sum_{n=0}^{N}\psi_n(z,n_0,t)X_n(\rho_C)\ , \tag{34}$$

with $C=A$ or B. [This approach leads to a separate wave packet for each possible electron vibrational eigenstate; the method is patterned after a similar basis-set or close-coupling expansion used in wave-packet treatments of molecular scattering. It is termed the "close-coupling wave packet" (CCWP) method.[19]] The analogous vector notation to Eq. (16) gives

$$\psi(z,n_0,t)=[\psi_0(z,n_0,t),\psi_1(z,n_0,t),\ldots,\psi_N(z,n_0t)]^T\ , \tag{35}$$

which satisfies

$$i\hbar\underline{I}\frac{\partial\psi}{\partial t}(z,n_0,t)=\underline{H}\psi(z,n_0,t)\ . \tag{36}$$

The formal solution is

$$\psi(z,n_0,t)=\exp(-it\underline{H}/\hbar)\psi(z,n_0,0)\ , \tag{37}$$

where $\underline{H}$ is still given by Eq. (18), and the initial wave packet has the form

$$[\psi(z,n_0,0)]_n=\delta_{nn_0}G(z)X_{n_0}(\rho_A)\ . \tag{38}$$

Thus, we begin the packet in the region $(-\infty,z_1)$ at a large enough z_0 so one has negligible overlap with the barrier region of the potential. The initial packet function $G(z)$ is taken to be

$$G(z)=(2\pi\sigma^2)^{-1/4}\exp\left[-\frac{(z-z_0)^2}{4\sigma^2}+ik_0(z-z_0)\right], \tag{39}$$

where $\hbar k_0/\mu$ is the group or average velocity and σ is the initial width parameter.

For a sufficiently short time step $t\equiv\tau$, one may utilize the symmetric split-operator (SSO) approximation[14–16] to write $\exp(-i\tau\underline{H}/\hbar)$ as

$$\exp(-\underline{H}\tau/\hbar)\cong\exp[-i\tau\underline{V}(z)/2\hbar]\exp\left[\frac{i\hbar\tau}{2\mu}\frac{\partial^2}{\partial z^2}\right]\times\exp[-i\tau\underline{V}(z)/2\hbar]\ . \tag{40}$$

The SSO approach to evaluating the action of the full

evolution operator can be based on the Baker-Hausdorff expansion of the exponential, $\exp(\sigma_1+\sigma_2)$, of a sum of noncommuting operators. Since the terms involving the nonvanishing commutators also contain powers of the times step τ, making τ small enough makes possible neglect of these terms. The symmetrized version, $\exp(\sigma_1/2)\exp(\sigma_2)\exp(\sigma_1/2)$, has its first nonvanishing commutator occurring with a higher power of τ than the unsymmetrized version, $\exp(\sigma_1)\exp(\sigma_2)$. In scattering problems, one typically writes $\exp(-iH\tau/\hbar)$ as $\exp(-iV\tau/2\hbar)\exp(-iK\tau/\hbar)\exp(-iV\tau/2\hbar)$, where K is the kinetic energy and V is the scattering potential. Then the action of $\exp(-iV\tau/2\hbar)$ is evaluated in the coordinate representation, while $\exp(-iK\tau/\hbar)$ is usually evaluated using the momentum representation, with the transformation between the two being achieved using fast Fourier transforms (FFT's).[14-16] The matrix $\exp[-i\tau\underline{V}(z)/2\hbar]$ can be calculated as

$$\{\exp[-i\tau\underline{V}(z)/2\hbar]\}_{nm}=\begin{cases}\delta_{nm}\exp\left[\dfrac{-i\tau}{2}(2n+1)\omega_A\right], & z\in A \quad (41a)\\ \exp\left[\dfrac{-i\tau}{2\hbar}V_0\right]\sum\limits_{m'}(\underline{A}^{-1})_{nm'}\exp\left[\dfrac{-i\tau}{2}(2m'+1)\omega_B\right](\underline{A})_{m'm}, & z\in B\ . \quad (41b)\end{cases}$$

The evaluation of the action of the free evolution operator, $\exp[(i\hbar\tau/2\mu)(\partial^2/\partial z^2)]$, can be carried out in a variety of ways, including the use of fast Fourier transforms[14,22] or the discrete distributed approximating function-effective free propagator.[17,23] Of course, one must test for convergence in the basis set by comparing results obtained with increasing numbers N of basis functions. When the results are stable with respect to increasing N, the calculation is assumed to be converged (provided that the results are also stable with respect to further refinement of other parameters, such as the time step τ, the grid size and grid increment in z, and the length of time propagation). The present calculations are believed to be converged to within a few percent. This is based, in part, on the level of agreement between the time-independent and time-dependent results. The former *only* depend on the number of vibrational basis functions, so that by refining the time step, grid size, length of propagation, and basis size, the two approaches have yielded results which are in reasonably good agreement (see Table II and Fig. 9).

The final stage of the time-dependent approach is the analysis to obtain the transmission and reflection amplitudes and probabilities at the collision energies of interest. By appropriate choice of the width and average momentum parameters σ and k_0 in Eq. (39), one can extract the scattering amplitudes at any desired energy. Furthermore, with reasonable choices of these parameters, results may be extracted over a very wide range of energies.[19,24,25] This is an extremely important feature of the wave-packet method because it means that wave packets that are relatively narrow in configuration space can be used to obtain results for many energies in a *single* wave-packet propagation. This includes any resonances that occur in the energy range described by the wave packet (although one must propagate the packet until all of the resonant portion has "leaked" out of the interbarrier region). In particular, as shown elsewhere,[19] it is *not* necessary to prepare wave packets that correspond to the narrow energy range of the resonance (and which then are extremely broad packets in coordinate space). However, the analysis in Cartesian coordinates should take account of the fact that in the initial packet, for any energy E, one has waves generated for both positive and negative momenta $\hbar k$. Previous studies have chosen σ and k_0 so as to minimize the contribution of the negative momenta.[19] We now give a procedure that allows one to determine the transmission and reflection amplitudes for an arbitrary initial wave packet $G(z)$. The basic idea to be used is that a second-order, ordinary, linear differential equation has two linearly independent solutions that can be taken to be both complex and complex conjugates of

TABLE II. Transmission and reflection coefficients for $n_0=0$, $E=1.919\times10^{-}$ eV.

n	$T(n_0,n,E)$[a]	% difference[b]	$T(n_0,n,E)$[c]	$R(n_0,n,E)$[a]	% difference	$R(n_0,n,E)$[c]
0	9.259×10^{-1}	3	9.530×10^{-1}	4.338×10^{-2}	8	3.974×10^{-2}
1	3.434×10^{-3}	4	3.563×10^{-3}	3.165×10^{-3}	2	3.692×10^{-3}
2	1.462×10^{-5}	4	1.515×10^{-5}	1.539×10^{-5}	3	1.588×10^{-5}
3	6.804×10^{-8}	4	7.049×10^{-8}	7.113×10^{-8}	3	7.347×10^{-8}
4	3.146×10^{-10}	4	3.261×10^{-10}	3.267×10^{-10}	3	3.380×10^{-10}
5	2.029×10^{-15}	10	2.240×10^{-15}	2.096×10^{-15}	10	2.311×10^{-15}

[a]CCWP.
[b]Computed as $|T(n,n_0,E)_{\rm CCWP}-T(n,n_0,E)_{\rm BM}|\times100/T(n,n_0,E)_{\rm CCWP}$.
[c]Boundary matching (BM).

one another. Then *any* solution of the equation can be expressed in terms of these two solutions. In a field-free region, these two solutions are $\exp(\pm ikz)$. A solution constructed from them could be labeled as an eigenstate of energy $E(=\hbar^2k^2/2m)$, even though it would no longer be an eigenstate of the linear momentum along z. In constructing the initial wave packet for this simple 1D scattering system, one would, in general, superpose both $\exp(ikz)$ and $\exp(-ikz)$, $k \geq 0$. Then when one analyzes the long-time wave packet, it is necessary to disentangle these two momentum components which contribute to the single energy $E=\hbar^2k^2/2m$ (i.e., one carries out a time-to-energy Fourier transform to extract the scattering at any particular energy, and this contains contributions from both the positive and negative initial momenta at the energy of interest). To carry out the disentangling analysis, one simply numerically evaluates the time-to-energy transform of the wave packet and makes use of the formal expression of the result as a sum (with as-yet-unknown coefficients) and the two linearly independent, complex solutions of the time-independent Schrödinger equation. This is done both in the reflected region ($z<z_1$) and the transmitted region ($z>z_4$) at a sufficient number of positions to generate the same number of equations as unknowns, these being the coefficients of the two linearly independent complex solutions of the Schrödinger equation at the energy of interest and the reflection and transmission amplitudes r and t. Since all are complex, there are a total of eight unknowns, and one uses the complex (numerical) value of the time-to-energy-transformed wave packet at four points, $\bar{z}_1$, $\bar{z}_2$, $\bar{z}_3$, and $\bar{z}_4$, to generate the required algebraic equations. Of course, in the present case there is also the additional electron-vibrational degree of freedom to consider. This leads to $2(N+1)$ linearly independent solutions of the time-independent coupled Schrödinger equations (since the solution is expanded in terms of $N+1$ vibrational basis functions). Since we only consider a *single* initial state for the wave packet, we in fact deal only with two of these linearly independent, complex solutions; namely, the two having the correct initial state for the electron vibration. It then follows that the same procedure as described above for the 1D electron-scattering problem can be applied separately to each of the possible final vibrational-state components of the wave packet.

We now consider the details for the present model of electron transmission and reflection in a 3D quantum wire. Note that

$$|\psi(n_0,E)\rangle=\frac{1}{2\pi\hbar}\int_{-\infty}^{\infty}dt\,e^{iEt/\hbar}e^{-iHt/\hbar}|\psi(n_0,0)\rangle\ , \tag{42}$$

where $|\psi(n_0,E)\rangle$ is the component of the wave packet associated with energy E. In the coordinate representation, it can be written as

$$\psi(z,r,n_0,E)=\sum_{n=0}^{N}X_n(\rho_C)\psi_n(z,n_0,E)\ , \tag{43}$$

where, unlike Eq. (15), the function $\psi_n(z,n_0,E)$ contains both $\psi_n^+(z,n_0,E)$ *and* its complex conjugate $[\psi_n^+(z,n_0,E)]^*$, since the complex solution of a second-order differential equation is linearly independent of its complex conjugate. Here, the plus (+) superscript denotes a solution of the time-independent Schrödinger equation in which the wave number k satisfying $\hbar^2k^2/2m=E$ is positive semidefinite. Returning to Eq. (42), we insert the resolution of the identity

$$1=\int_0^{\infty}dE'\left[\psi^+(z,r,N_0,E')\int_{-\infty}^{\infty}dz'\int_0^{\infty}dr'r'(\psi^+(z',r',n_0,E'))^*\right.$$
$$\left.+(\psi^+(z,r,n_0,E'))^*\int_{-\infty}^{\infty}dz'\int_0^{\infty}dr'r'\psi^+(z',r',n_0,E')\right] \tag{44}$$

into Eq. (42), noting that

$$H\psi^+(z,r,n_0,E')=E'\psi^+(z,r,n_0,E') \tag{45}$$

and

$$H(\psi^+(z,r,n_0,E'))^*=E'(\psi^+(z,r,n_0,E'))^*\ . \tag{46}$$

Using the fact that

$$\frac{1}{2\pi\hbar}\int_{-\infty}^{\infty}dt\,e^{iEt/\hbar}e^{-iE't/\hbar}=\delta(E-E')\ , \tag{47}$$

we obtain

$$\psi(z,r,n_0,E)=\psi^+(z,r,n_0,E)\int_{-\infty}^{\infty}dz'\int_0^{\infty}dr'r'[\psi^+(z',r',n_0,E)]^*\psi(z',r',n_0,0)$$
$$+[\psi^+(z,r,n_0,E)]^*\int_{-\infty}^{\infty}dz'\int_0^{\infty}dr'r'\psi^+(z',r',n_0,E)\psi(z',r',n_0,0)\ . \tag{48}$$

We project Eq. (48) onto one of the final vibrational states of the electron at four selected points $z=\bar{z}_1$, $\bar{z}_2$, $\bar{z}_3$, and $\bar{z}_4$, two of which are chosen to be in the region $(-\infty,z_1)$ and two in (z_4,∞), with $\bar{z}_1$ and $\bar{z}_2$ close to z_1 and $\bar{z}_3$ and $\bar{z}_4$ close to z_4. (It is found that the computational results are not sensitive to the precise values of the $\bar{z}_j$, $j=1-4$, provided they are in the regions indicated.) Then by Eqs. (43) and (48), we find

$$\psi_n(\bar{z}_j,n_0,E)=C(n_0,E)\psi_n^+(\bar{z}_n,n_0,E) +D(n_0,E)[\psi_n^+(\bar{z}_j,n_0,E)]^* , \quad (49)$$

with

$$C(n_0,E)\equiv\int_{-\infty}^{\infty}dz'\int_0^{\infty}dr'r'[\psi^+(z',r',n_0,E)]^* \times\psi(z',r',n_0,0) \quad (50)$$

and

$$D(n_0,E)\equiv\int_{-\infty}^{\infty}dz'\int_0^{\infty}dr'r'\psi^+(z',r',n_0,E) \times\psi(z',r',n_0,0) . \quad (51)$$

Note that Eqs. (49)–(51) simply express the fact that the complex solution of the Schrödinger equation at energy E, with positive wave number k ($\hbar^2k^2/2m=E$), and its complex conjugate are linearly independent and together can be used to express the nth component of the wave packet at energy E. Of course, $C(n_0,E)$, $D(n_0,E)$, $\psi_n^+(\bar{z}_j,n_0,E)$, and $[\psi_n^+(\bar{z}_j,n_0,E)]^*$ are all unknown, and $\psi_n(\bar{z}_j,n_0,E)$ is computed as the time-to-energy transform of the wave-packet projection $\psi_n(z,n_0,t)$; see Eq. (34). One may now make use of the known form of $\psi_n^+(z,n_0,E)$ in terms of the $r(n,n_0)$ and $t(n,n_0)$, so that by combining Eqs. (22a), (22b), and (49), we have

$$\psi_n(\bar{z}_j,n_0,E)=C(n_0,E)[\delta_{nn_0}e^{ik_n\bar{z}_j}+r(n,n_0)e^{-ik_n\bar{z}_j}] +D(n_0,E)[\delta_{nn_0}e^{-ik_n\bar{z}_j}+r^*(n,n_0)e^{ik_n\bar{z}_j}] , \quad (52)$$

with $\bar{z}_j$ equal to $\bar{z}_1$ or $\bar{z}_2$, and

$$\psi_n(\bar{z}_j,n_0,E)=C(n_0,E)t(n,n_0)e^{ik_n\bar{z}_j} +D(n_0,E)t^*(n,n_0)e^{-ik_n\bar{z}_j} , \quad (53)$$

with $\bar{z}_j$ equal to $\bar{z}_3$ or $\bar{z}_4$. Now the unknowns, $C(N_0,E)$, $D(n_0,E)$, $r(n,n_0)$, and $t(n,n_0)$ are complex, so there are eight unknowns in the set of equations above. There are four values of $\bar{z}_j$, and each gives rise to two equations, since $\psi_n(\bar{z}_j,n_0,E)$ are complex. There are, therefore, the same number of equations as unknowns, and it is straightforward, but tedious, to solve them. Note that one *cannot* use a standard linear algebra procedure because the equations are nonlinear. However, note also that $C(n_0,E)$ and $D(n_0,E)$ are *independent* of n. Thus, once they are determined (e.g., by solving the equations with n set equal to n_0), the remaining equations are linear. Thus, one may solve the subsequent equations for $n\neq n_0$ by efficient linear algebra codes. This completes the discussion of the methods used in this study.

III. COMPUTATIONAL RESULTS AND ANALYSIS

We first give a tabular comparison of results obtained by both the time-independent boundary matching procedure and the time-dependent CCWP approach. The values of the parameters used in the CCWP calculation are given in Table I. It is to be noted that the double barrier along z presents a challenging calculation because flux can become trapped in the well created by the two juxtaposed barriers. The calculation involves 38 506 time steps, each of 1 fs, for a total time of 38.506 ps. The time propagation has been continued long enough so that the remaining wave-packet amplitude between the two barriers is negligibly small. The results (both obtained by the time-independent, linear algebraic method and the wave-packet method) at an energy equal to $\frac{1}{2}$ the barrier height (this energy coincides with a strong resonance in transmission) are given in Table II, and we see that generally most transition probabilities agree to 3% or 4%, with the exception of the transmission and reflection of the electron accompanied by the vibrational transition $0\rightarrow5$ and the vibrationally elastic reflection. In the case of the $0\rightarrow5$ vibrational transition, the probability is so small as to be totally unimportant. In the case of the $0\rightarrow0$ reflection, most of the difference is associated with the fact that the $0\rightarrow0$ transmisson differs by 3% for the two methods, and since that probability is the largest by far, it strongly affects the $0\rightarrow0$ reflection. This indicates satisfactory agreement between the two totally different methods.

Of more interest than results at a single energy, of course, are results over a wide range of energies. This allows one to explore conditions under which the electron makes the switch from reflection to transmission, and especially resonant transmission. Results are shown in Fig. 2 for the case $\omega_A=\omega_B$. Of course, in this case, there is no coupling in the electron vibration, and one simply

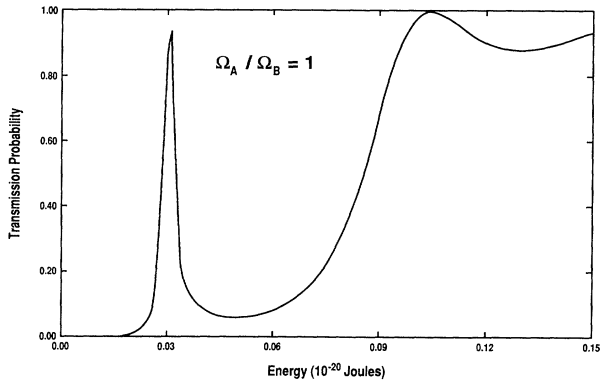

FIG. 2. Transmisison probability for the frequency ratio $\omega_A/\omega_B=1$ (effective 1D tunneling through a double barrier). Barrier height $V_0=6.1476\times10^{-20}$ J. The $n=0\rightarrow1$ transmission probability is zero.

has scattering by a double barrier. The cylindrical symmetry with zero initial angular momentum, combined with zero vibrational coupling, makes this case effectively a 1D problem, and this is clearly shown in the typical form of the transmission probability as a function of energy. There appears to be a strong resonance when the energy is about $\frac{1}{2}$ the height of the two barriers. A second resonance occurs somewhat higher up. As we shall see, these effective 1D results are also useful in interpreting the results when $\omega_A \neq \omega_B$ leads to vibrational excitation of the electron. We emphasize that the results over the whole energy range were gotten from a *single* wave-packet propagation, including those at the narrow resonance.

An interesting question to explore is the effect on the vibrational transitions and transmission of varying ω_A and ω_B. From the form of the coupling in the potential, Eqs. (13) and (21) (which arises from the discontinuous change in the electron vibrational frequency), we note that if $\omega_B \gg \omega_A$, then $\gamma \cong 1$ and $\sqrt{\omega_A \omega_B}/(\omega_A + \omega_B)$ is approximately $\sqrt{\omega_A/\omega_B}$. Conversely, if $\omega_A \gg \omega_B$, then $\gamma \cong -1$ and $\sqrt{\omega_A \omega_B}/(\omega_A + \omega_B)$ is approximately $\sqrt{\omega_B/\omega_A}$. Now, as either ω_A or ω_B gets very large relative to the other, the matrix elements $(\underline{A})_{nm}$ become small due to the hypergeometric function being well behaved for $\gamma = \pm 1$. Thus, the unitarity of $\underline{A}$, combined with the $\sqrt{\omega_A/\omega_b}$ $(\gamma = +1)$ or $\sqrt{\omega_B/\omega_A}$ $(\gamma = -1)$ behavior leads to the coupling becoming small between any pair of states; i.e., the coupling is dispersed widely among the vibrational states. Within the truncated basis, this will lead to effective decoupling of the vibrational states. Physically, this limit reflects the effect of the mismatch of energy levels. A related question of interest is whether vibrational inelasticity will be enhanced when certain energy levels in region B coincide with final levels in region (z_4, ∞). For $n_0 = 0$, the lowest condition for inelastic energy resonance is to the $n = 1$ final state in region (z_4, ∞). The energy resonance condition is then

$$(2m+1)\omega_B = 3\omega_A \ , \tag{54}$$

which leads to the condition $\omega_A/\omega_B = (2m+1)/3$. The lowest-energy resonance has $m = 0$ in the B region, and the ratio for this is

$$\omega_A/\omega_B = \tfrac{1}{3} \ . \tag{55}$$

When $m = 1$, obviously resonance implies $\omega_A \equiv \omega_B$, and no transition occurs. One only gets resonance for ω_A/ω_B ratios equal to ratios of odd integers. If the final vibrational state is $n = 2$, the lowest-energy resonance occurs again for $m = 0$ and a ratio

$$\omega_A/\omega_B = \tfrac{1}{5} \ . \tag{56}$$

We expect from this sort of analysis, and that for $\omega_A \rightarrow$ large, that ratios of ω_A/ω_B that are larger than one are unfavorable to inelasticity. We have carried out calculations to explore these ideas. In Figs. 3 and 4 we show results for $\omega_A/\omega_B = 2$ and 3, respectively. The first case clearly does not correspond to any matching of energy levels between regions A and B, and we see that very little excitation of the electron vibration occurs. The shape and location of resonant transmission is very close to that for the effective 1D case. The $n = 0 \rightarrow 1$ vibrational excitation transmission probability is larger for the case $\omega_A/\omega_B = 3$, but still is very small. This seems consistent with the fact that the $m = 1$ level of the B-region oscillation matches the $n = 0$ level of region A, and $m = 0$ does not match any level in region A, so the vibrationally adiabatic transmission is favored. The shape and location of resonant transmission again closely correspond to the effective 1D case.

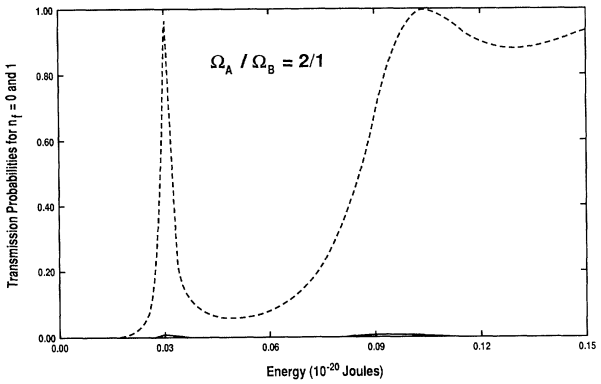

FIG. 3. Same as Fig. 2, except $\omega_A/\omega_B = 2/1$. The transmission probability with $n = 0 \rightarrow 1$ (solid curve) is very small but nonzero. The dashed curve is for $n = 0 \rightarrow 0$.

In Figs. 5–9 we present results for cases where $\omega_A/\omega_B < 1$. The first case is for $\omega_A/\omega_B = \frac{3}{4}$, which we again expect will be very similar to the effective 1D case $\omega_A = \omega_B$. This is borne out by the results shown in Fig. 5. In Fig. 6, the ratio is taken to be $\omega_A/\omega_B = \frac{1}{2}$. Although this is not a resonant ratio, it does produce larger vibrational coupling matrix elements and is moving closer to the first resonant case of $\omega_A/\omega_B = \frac{1}{3}$, and we see a substantial increase in transmission for which the electron has been vibrationally excited to $n = 1$. However, although there is a slight shift to higher energy, the basic shape and location of peaks in the transmission probabili-

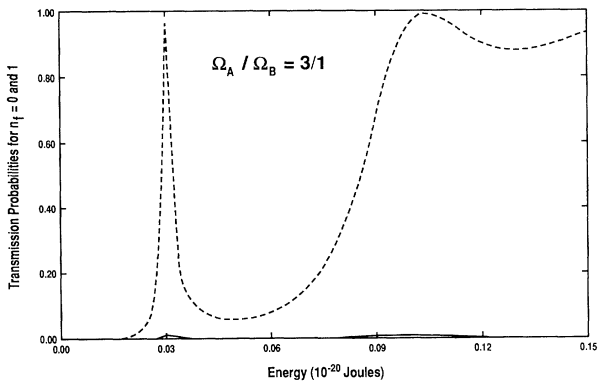

FIG. 4. Same as Fig. 2, except $\omega_A/\omega_B = 3/1$. The transmission probability with $n = 0 \rightarrow 1$ (solid curve) is very small but nonzero. The dashed curve is for $n = 0 \rightarrow 0$.

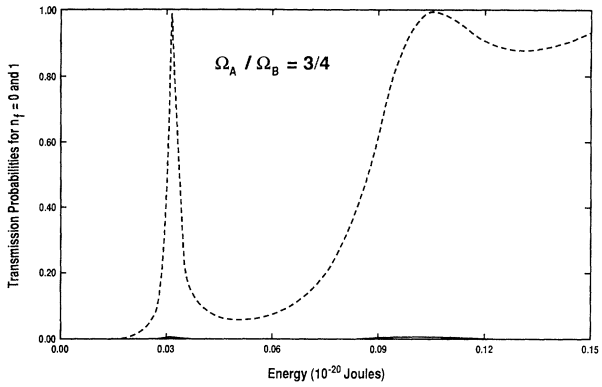

FIG. 5. Same as Fig. 2, except $\omega_A/\omega_B = \frac{3}{4}$. The vibrationally inelastic probability is very small but nonzero. The dashed curve is for $n = 0 \rightarrow 0$, and the solid curve is for $n = 0 \rightarrow 1$.

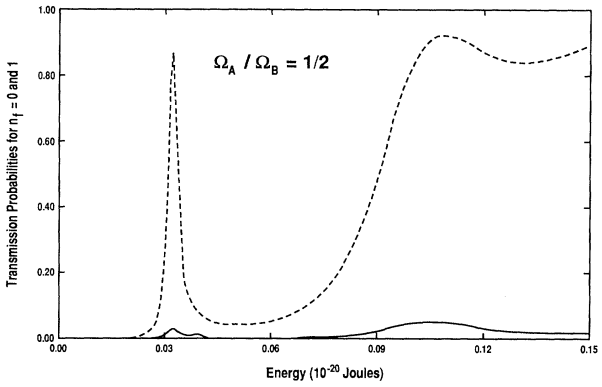

FIG. 6. Same as Fig. 2, except $\omega_A/\omega_B = \frac{1}{2}$. The $n = 0 \rightarrow 1$ (solid curve) inelastic transmission probability is small but substantially larger than for larger ratios of ω_A/ω_B.

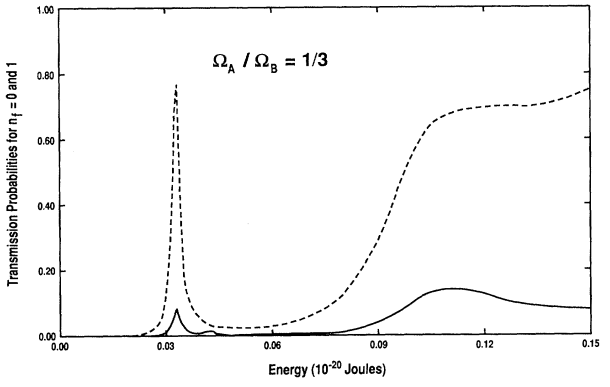

FIG. 7. Same as Fig. 2, except $\omega_A/\omega_B = \frac{1}{3}$. The $n = 0 \rightarrow 1$ (solid curve) transmission probability is now significant, though still smaller than the vibrationally elastic transmission. For this ratio of ω_A/ω_B, the $n = 1$ level in A equals the $m = 0$ level in B.

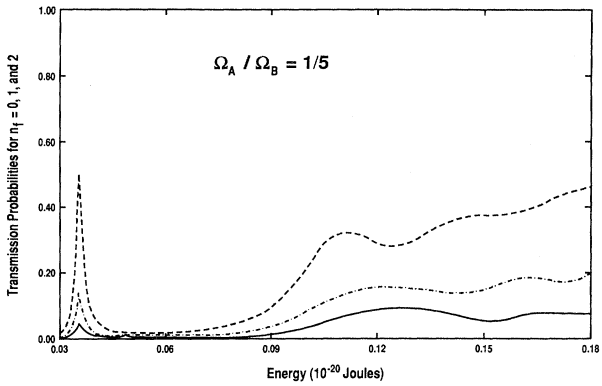

FIG. 8. Same as Fig. 2, except $\omega_A/\omega_B = \frac{1}{5}$. The $n = 0 \rightarrow 2$ transmission probability is now significant, although still smaller than the $n = 0 \rightarrow 1$. For this ratio of ω_A/ω_B, the $n = 2$ level in A equals the $m = 0$ level in B. The dashed curve is $n = 0 \rightarrow 0$, the dashed-dotted curve is for $n = 0 \rightarrow 1$, and the solid curve is for $n = 0 \rightarrow 2$.

ty still clearly correspond to the effective 1D situation.

Figure 7 shows the results for the lowest resonant matching case of $\omega_A/\omega_B = \frac{1}{3}$, which corresponds to matching the $m = 0$ level of the B-region electron vibration with the $n = 1$ level of the electron vibration in region (z_4, ∞). It also leads to larger coupling between different vibrational levels in regions A and B. There has clearly been a considerable increase in vibrational excitation accompanying transmission of the electron through the double-barrier region. The shape and location of the major peaks in the transmission probability are still strongly correlated to the effective 1D case. There is, however, also now the beginning of a small satellite peak occurring just a little higher in energy than the lowest peak. In addition, there is a small but significant shift to higher energy of the dominant transmission peaks. This reflects the effect of internal coupling of the vibration on the resonant transmission levels.

In Fig. 8, we display results for the ratio $\omega_A/\omega_B = \frac{1}{5}$, which corresponds to a match of the $n = 2$ level of the electron oscillation in region (z_4, ∞), with the $m = 0$ level in the B region. In this case, we have extended the calculations to substantially higher energies, which shows the

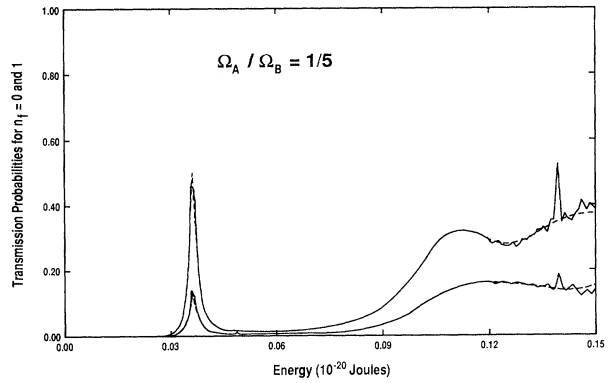

FIG. 9. Same as Fig. 8 except results obtained by the CCWP time-dependent method (dashed curve) are compared to the BM time-independent method (solid curve).

additional oscillations arising due to the intermittant occurrence of resonant transmission in the underlying effective 1D problem. Of greatest interest are the facts that (a) the shift to higher energy of the resonances is now pronounced and (b) the satelite peak is smaller, but more separated at higher energy, while (c) the excitation into the $n=2$ final state of the electronic vibration is still significant (and in fact is larger than it was for $\omega_A/\omega_B=\frac{1}{3}$); the $n=0\rightarrow n=1$ transmission probability remains the largest. It also is the transition with the largest coupling in the $\underline{A}$ matrix. Thus, although there appears to be an effect of "frequency matching," the dominant physical effect controlling the magnitude of vibrational transition probability in the electron transmission in the present model system is the size of the coupling overlap matrix elements.

In Fig. 9 we show a comparison of results obtained using the CCWP and boundary-matching (BM) methods for the $\omega_A/\omega_B=\frac{1}{5}$ case. While they are seen to match for energies below about 10^{-21} J, *the BM results become unstable at higher energies.* The CCWP method, by contrast, continues to work well, providing smooth results from a little less than 3×10^{-22} J up to 1.8×10^{-21} J in a single-wave-packet propagation. This is extremely encouraging, since we plan to consider substantially more complicated models for electron transmission in nanostructures, and the CCWP time-dependent method should handle them readily.

Finally, we note that the parameters used in our model are such as to make the present study complementary to that of Bryant.[20] He also found that vibrational coupling ("mode mixing") affects the amount of transmission at resonances, and he directly varied an overlap parameter β in order to study the effects of varying the amount of mode mixing. In our study, we focus on varying the ratio of the harmonic transverse (radial) vibrational frequencies of regions A and B, which by Eqs. (13) and (14) determine the values of our overlap matrix elements. We and Bryant see the appearance of "satellite resonance peaks" (fine structure) when the vibrational transition probability increases. Bryant obtained results including a total of four lateral vibrational states, and in each region the harmonic frequency is the same for both x and y motion (square symmetry). In our study, the coupling is such that a total of ten transverse (radial) vibrational states are included, but due to cylindrical symmetry only the magnetic quantum state $m=0$ is included. Thus, Bryant includes what are effectively states of nonzero electronic angular momentum, but he includes substantially fewer vibrational states. For certain cases, Bryant encountered difficulties in maintaining a unitary scattering matrix, and imposed this externally. We found that our time-dependent CCWP method produced accurate, unitary results over the entire range of energies studied, without requiring any additional unitarization procedures. Finally, we, like Bryant, find that vibrational transitions occur principally in the resonance tunneling energy regimes.

IV. CONCLUSIONS

A 3D model simulating electron tunneling in a quantum wire has been studied computationally by two totally different numerical methods. Numerical solutions of the time-independent Schrödinger equation were obtained using a multichannel analogue of the standard boundary-matching procedure commonly used in the solution of "textbook" problems of tunneling in one dimension.[20] The close-coupling wave-packet approach was used to calculate solutions to the time-dependent Schrödinger equation for the same model, and a new procedure developed for extracting the transmission and reflection amplitudes. Comparison of results obtained by the methods were found to agree within a few percent, except for medium to higher energies. For this range of energy, reliable results were obtained only by the CCWP approach. Convergence of our results with respect to basis-set size was confirmed in calculations including up to 15 vibrational eigenstates. Production runs were made using ten vibrational eigenstates. Convergence with respect to other parameters was also confirmed by comparison to more refined parameter set calculations.

The simplicity of the model enabled us to carry out straightforward analysis of the coupling which was responsible for causing transitions in the electron's vibration transverse to the axis of the quantum wire. When the electron's oscillation frequency was the same in regions A and B, the symmetry of the model makes it effectively a 1D tunneling problem. The resulting transmission probability was that of a 1D double-barrier problem. This basic structure of the transmission probability was found to be present for all cases of vibrational coupling considered. The peaks in the transmission probability curves, however, shift toward higher energies as the amount of vibrational excitation increases for the $\omega_A\neq\omega_B$ cases. In addition, satellite peaks occur for the case involving higher amounts of vibrational transitions.

The dominant effect controlling the probability of transmission accompanied by vibrational excitation of the electron is the size of the overlap between the vibrational states in region B with various initial and final vibrational states of the electron in region A. Also of interest is the role of the ratio of the oscillator frequencies in the two regions. Accidental degeneracy occurs when the ratio ω_A/ω_B equals the ratio of two odd integers. The lowest-energy matching occurs for $\omega_A/\omega_B=\frac{1}{3}$ and $\frac{1}{5}$, the former leading to significant transmission accompanied by the $n=0\rightarrow1$ transition, and the latter also involving $n=0\rightarrow2$ (as well as $n=0\rightarrow1$, which is the largest due to the largest overlap).

Our results are consistent with those found in an earlier study by Bryant (also, using a time-independent BM method).[20] The model parameters (which are consistent with what can be fabricated experimentally by MBE) and basis-set sizes make the present study complementary to that of Bryant.

ACKNOWLEDGMENTS

X.M. and D.J.K. were supported in part by the R.A. Welch Foundation (Grant. No. E-608). Ames Laboratory is operated for the Department of Energy by Iowa State University under Contract No. 2-7405-ENG82.

[1]See, e.g., R. T. Bate, Trends Comput., March (1988); R. T. Bate, G. Frazier, W. Frensley, and M. Reed, Texas Instrum. Tech. J., July-August (1989).
[2]L. L. Chang, I. Esaki, and R. Tsu, Appl. Phys. Lett. **24**, 593 (1974).
[3]T. C. L. G. Sollner, W. D. Goodhue, P. E. Tannenwald, C. D. Parker, and D. D. Peck, Appl. Phys. Lett. **43**, 588 (1983).
[4]*Nanostructure Physics and Fabrication,* edited by M. A. Reed and W. P. Kirk (Academic, New York, 1989).
[5]*Physics and Technology of Submicron Structures,* edited by H. Heinrich, G. Bauser, and F. Kuchar (Springer, New York, 1988).
[6]J. H. Luscombe and W. R. Frensley, Nanotech. **1**, 131 (1990).
[7]B. P. van der Gaas and A. Scherer, Appl. Phys. Lett. **56**, 481 (1990).
[8]J. N. Randall, M. A. Reed, J. H. Luscombe, G. A. Frazier, W. R. Frensley, Y. C. Kao, T. M. Moore, and R. J. Matyi (unpublished).
[9]T. J. Thornton, M. Pepper, H. Ahmed, D. Andrews, and G. J. Davies, Phys. Rev. Lett. **56**, 1198 (1986).
[10]H. van Houten, B. J. van Wees, M. G. J. Heijman, and J. P. Andere, Appl. Phys. Lett. **49**, 1781 (1986).
[11]G. Timp, A. M. Chang, P. Mankiewich, R. Behringer, J. E. Cunningham, T. Y. Chang, and R. E. Howard, Phys. Rev. Lett. **59**, 732 (1987).
[12]M. A. Reed, J. N. Randall, R. J. Aggerwal, R. J. Matyi, T. M. Moore, and A. E. Wetsel, Phys. Rev. Lett. **60**, 535 (1988).
[13]J. N. Randall, M. A. Reed, T. M. Moore, R. J. Matyi, and J. W. Lee, J. Vac. Sci. Technol. **136**, 302 (1988).
[14]M. D. Feit and J. A. Fleck, Jr., J. Chem. Phys. **79**, 301 (1983); **80**, 2578 (1984).
[15]P. DeVries, in *Atomic and Molecular Processes with Short Intense Laser Pulses,* Vol. 171 of *NATO Advanced Study Institute, Series B: Physics,* edited by A. D. Bandrauk (Plenum, New York, 1987), p. 113.
[16]A. D. Bandrauk and H. Shen, Chem. Phys. Lett. **176**, 428 (1991).
[17]D. K. Hoffman, N. Nayar, O. A. Sharafeddin, and D. J. Kouri, J. Phys. Chem. **95**, 8299 (1991).
[18]D. K. Hoffman, M. Arnold, and D. J. Kouri (unpublished).
[19]R. C. Mowrey and D. J. Kouri, J. Chem. Phys. **84**, 6466 (1986); **86**, 6140 (1987).
[20]G. W. Bryant, Phys. Rev. B **39**, 3145 (1989); **44**, 3782 (1991); **44**, 12 837 (1991).
[21]*Handbook of Mathematical Functions,* edited by M. Abramowitz and I. A. Stegun (Dover, New York, 1964).
[22]D. Kosloff and R. Kosloff, J. Comput. Phys. **52**, 35 (1983); J. Chem. Phys. **79**, 1823 (1983).
[23]N. Nayer, D. K. Hoffman, X. Ma, and D. J. Kouri (unpublished).
[24]D. K. Hoffman, O. A. Sharafeddin, R. S. Judson, and D. J. Kouri, J. Chem. Phys. **92**, 4167 (1990); O. A. Sharafeddin, D. J. Kouri, R. S. Judson, and D. K. Hoffman, *ibid.* (to be pulished).
[25]D. Neuhauser, J. Chem. Phys. **93**, 2611 (1990); **93**, 7836 (1990).